ACS OMEGA

http://pubs.acs.org/journal/acsodf

Article

Suppression of Brake Noise and Vibration Using Aramid and Zylon Fibers: Experimental and Numerical Study

Navnath Kalel, Bhaskaranand Bhatt, Ashish Darpe, and Jayashree Bijwe*

Cite This: *ACS Omega* 2022, 7, 21946−21960

Read Online

ACCESS | Metrics & More | Article Recommendations

ABSTRACT: Aramid pulp/fiber is the most vital ingredient of brake friction material (FM) formulation. It is perpetually added to achieve quality brake pads/shoes and improve the overall friction and wear performance. Additionally, novel Zylon fibers have a superior property to aramid fibers. However, no studies give insights on their influence on brake noise and vibration (NV) performance. In the current work, a series of six different types of eco-friendly brake pads was developed. The first five contain aramid pulp, aramid short fibers, and Zylon fibers of different sizes (1, 3, and 6 mm) as the theme ingredients (3 wt %) by keeping the parent composition identical. Additionally, one more pad was developed that contains no aramid/Zylon fibers (i.e., reference pad). The pads were characterized for physical and mechanical properties. The damping and natural frequencies of pads were measured experimentally and numerically. All brake pads were evaluated for detailed NV performance by following the SAE J 2521 test schedule. In addition, numerical simulation was performed to validate the experimental brake squeal results. Results revealed that aramid/Zylon fiber-based pads improved the porosity, damping, and compressibility. Overall, brake noise and vibrations were improved for aramid/Zylon fiber-based pads by 1.2−1.5 dBA and 20−25%, respectively, compared to the reference pad. The complex eigenvalue analysis (CEA) proved that squeal was mainly influenced by the damping and density of the pad materials. Thus, aramid/Zylon fiber-based pads can effectively suppress the instability of the brake system and reduce the brake squeal propensity.

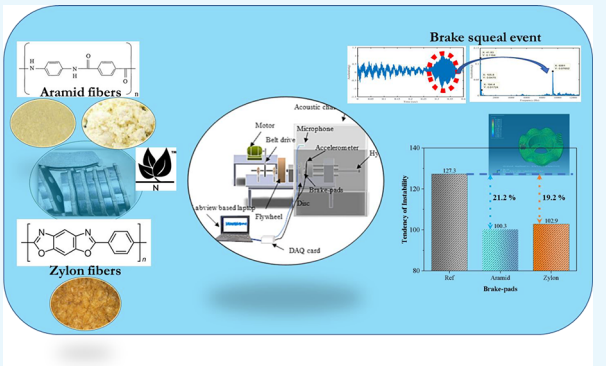

1. INTRODUCTION

The brake is a crucial member of an automobile that ensures operational safety for a wide range of operating conditions. With brake noise pollution and related customer dissatisfaction, several attempts have been made to predict and eliminate the brake noise issues by the researchers. In general, brake noise is classified into various categories depending upon the frequency ranges, such as judder (<100 Hz), groan (<500 Hz), moan (<500 Hz), howl (500 Hz to 1 kHz), wire brush (>1 kHz), squeal (>1 kHz), etc.[1−4] The friction-induced vibration brake noise problems were widely studied in the 20th century and summarized in review articles.[1,2] Several researchers have studied brake squeal problems using experimental[5−13] and numerical[14−22] techniques in the past decades. Generally, the design is first determined by the brake pad/lining materials in the brake industry due to their main role in the braking performance and the squeal propensity. However, unfortunately, the composition and material properties of brake pad/lining materials usually considered proprietarily are not known in specific details. Generally, changing the pad/lining materials, using a damping shim, and modifying the pad/lining/disc geometry are common ways to minimize brake noise and vibration issues.[23,24]

Recently, a few researchers have attempted to minimize the brake noise by changing the brake pad's composition. Brake squeal is strongly associated with the natural frequencies of the key components of the brake system, i.e., the brake pad and disc.[25−27] For instance, Masoomi et al.[28] studied the role of thermoplastic elastomer (TPE) ingredients in friction materials (FMs), and the results suggested that damping properties can be strongly affected by TPE and the high content of TPE proved to be the best for noise reduction. Bhatt et al.[29] explored the potential of calcium silicate (commercially Promaxon-D) to ameliorate the brake noise and vibration (NV) performance. Results revealed that 20 wt % Promaxon-D in Cu-free brake pads proved to be the best for the overall NV performance. Kalel et al.[30] studied the role of different types of stainless-steel particles (SSPs) on brake NV performance, and a comparative study was

Received: April 13, 2022
Accepted: June 2, 2022
Published: June 10, 2022

done with a Cu particle-based pad. Results showed a marginal difference in NV performance of pads, and one of the investigated SSPs can be a suitable choice in Cu-free pads. Kamioka et al.[31] revealed cashew dust and rubber particles in the brake pads, which proved to be beneficial in suppressing the noise due to their superior viscoelastic properties. Yamashita et al.[31−33] reported that mica and vermiculite are commonly used as fillers in brake pads/shoes, reducing the low-frequency noise due to the needle-like structure and porosity.

Aramid in pulp form is an almost inevitable ingredient of good-quality non-asbestos organic (NAO) friction materials (FMs). It provides better processability, sufficient strength to preform, stability in μ, and increased resistance to fade and wear of FMs.[34−39] Although aramid fibers/pulp is explored extensively in the brake pads for improving the tribological performance, no studies are available on the role of aramid fibers/pulp on brake NV performance. In contrast, Zylon fibers (i.e., PBO: *p*-phenylene-2,6-benzobisoxazole) have superior properties (1.6 times higher tensile strength, Young's modulus, thermal stability, etc.) to aramid fibers.[40] But, it has not been explored yet in brake pads.

Based on the important aspects of materials for brake NV performance, in the current work, a series of six types of brake pads was developed. The first five contain aramid pulp, short aramid fibers (1 mm), and Zylon fibers with varying lengths (i.e., 1, 3, and 6 mm) as the theme ingredients (3 wt %) by keeping the parent composition identical. The selected theme ingredient content (3 wt %) was based on the previous studies.[29,30,36,37,50,51] One more type of brake pad was developed without aramid/Zylon fibers (reference pad) for comparison. The detailed comparative noise and vibration studies were carried out, and the results are compiled and discussed in the subsequent sections.

2. MATERIALS AND METHODOLOGY

2.1. Materials and Fabrication of Brake Pads. The developed brake pad composition consists of a total of 13 ingredients, including the theme ingredient. A series of six Cu-free (low metallic) brake pads was developed. The first five types of pads were based on theme ingredients (3 wt %), aramid/Zylon fibers, by keeping the parent composition identical. As mentioned earlier, an additional pad was developed without the theme ingredient (i.e., a reference pad). The development process of the brake pads is reported in the earlier work.[41,42] The composition and designation of developed brake pads in the laboratory are summarized in Table 1.

Table 1. Composition and Designation of Developed Brake Pads[b]

ingredient (wt %)	designation of brake pads					
	Ref	AP	AF_1	Z_1	Z_3	Z_6
parent composition[a]	75	75	75	75	75	75
aramid/zylon fibers (theme ingredient)	0	3/0	3/0	0/3	0/3	0/3
space filler (barite)	25	22	22	22	22	22

[a]Parent composition (75 wt %): binder:organic fibers:friction modifier:fillers, 6:13:12:44. [b]Ref, brake pad without aramid/Zylon fibers; AP, aramid pulp-based brake pad; AF_1, aramid (1 mm) fiber-based brake pad; Z_1, Zylon (1 mm) fiber-based brake pad; Z_3, Zylon (3 mm) fiber-based brake pad; Z_6, Zylon (6 mm) fiber-based brake pad.

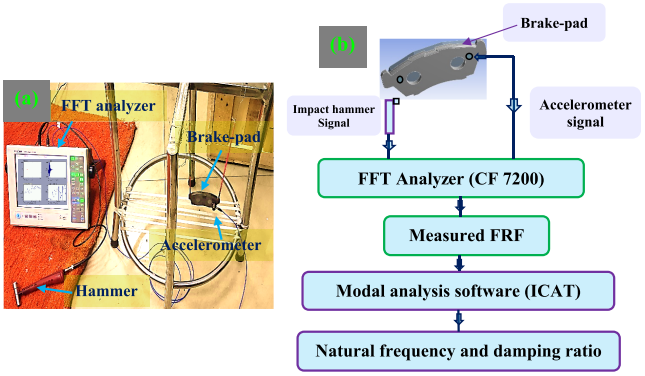

Figure 1. (a) Experimental test setup. (b) Schematic diagram of the modal analysis procedure.

2.2. Characterizations of Brake Pads. The developed brake pads were characterized for physical (density and porosity) and mechanical (hardness and compressibility) properties as per the standards. The density was measured as per the Archimedes principle, porosity (JIS D 4418), hardness (ASTM D 785), and compressibility (ISO 6310) standards. Each test was done five times, and the average values of results are reported.

2.3. Modal Analysis of Brake Pads. The experimental modal analysis helps evaluate the parameters of a mechanical vibratory system and gives information of its natural frequencies, mode shapes, and damping ratios. The experimental modal analysis and numerical eigenvalue analysis were carried out for the brake disc and brake pads.

2.3.1. Experimental Technique. This subsection describes the experimental modal analysis of the developed brake pads and the brake disc to obtain the natural frequencies and damping ratio. Figure 1 shows the experimental test setup and schematic diagram of the test procedure.

The damping property of a structure plays a vital role in controlling its noise and vibration characteristics. Experimental modal analysis is carried out by simultaneous measurement of the input excitation force and the output vibration response to get the frequency response function (FRF). A fast Fourier transform (FFT) analyzer (model CF 7200, ONO SOKKI, Japan) was used to acquire the impact hammer (model 8206, B&K, Denmark) and accelerometer (model 352C03, PCB Piezoelectronics, USA) signals and compute the corresponding FRF. The acquired raw data is then input to the ICAT modal analysis software. In ICAT software, the circle fit method was used to find the natural modes and the corresponding natural frequency and damping ratio for the disc and brake pads. The several sets of measurement data of force excitation and vibration were recorded using a modal hammer and accelerometer, and corresponding FRFs were found for disc and each type of brake pad. In the present work, the measurements were done in a free-free condition of the pad samples (Figure 1a) to avoid the influence of the boundary conditions (say, support clamping force) on the modal properties of the sample.

2.3.2. Numerical Modal Analysis. The mode shapes and natural frequencies for the disc and developed brake pads were also studied in ANSYS19 software. To match the free-free boundary conditions used in the experimental measurements, the same boundary conditions were applied in the simulations. The finite element models of the disc and pad were constructed

https://doi.org/10.1021/acsomega.2c02313
ACS Omega 2022, 7, 21946−21960

Table 2. Convergence Analysis of Disc and Brake Pad Sample FE Models for Different Element Sizes, Numbers of Elements, and Nodes[a]

	disc			brake pad sample		
element size (mm)	number of nodes (N) and elements (E)	natural frequencies (Nf), (Hz)	% change in NF with a reduction in element size	number of nodes (N) and elements (E)	natural frequencies (Nf), (Hz)	% change in Nf with a reduction in element size
4 mm	N, 21118; E, 11257	Nf_1, 1755; Nf_2, 3347; Nf_3, 4972; Nf_4, 6971		N, 1312; E, 196	Nf_1, 9940; Nf_2, 12168; Nf_3, 13229; Nf_4, 13956	
3 mm	N, 36471; E, 19905	Nf_1, 1729; Nf_2, 3335; Nf_3, 4957; Nf_4, 6957	Nf_1, 1.48; Nf_2, 0.36; Nf_3, 0.30; Nf_4, 0.20	N, 2460; E, 405	Nf_1, 9938; Nf_2, 12166; Nf_3, 13220; Nf_4, 13956	Nf_1, 0.02; Nf_2, 0.02; Nf_3, 0.07; Nf_4, 0.03
2 mm	N, 81245; E, 45362	Nf_1, 1726; Nf_2, 3326; Nf_3, 4947; Nf_4, 6945	Nf_1, 1.65; Nf_2, 0.63; Nf_3, 0.50; Nf_4, 0.37	N, 6412; E, 1183	Nf_1, 9754; Nf_2, 12095; Nf_3, 13072; Nf_4, 13929	Nf_1, 1.87; Nf_2, 0.66; Nf_3, 1.19; Nf_4, 0.22

[a]N, nodes; E, elements; Nf, natural frequency (Hz).

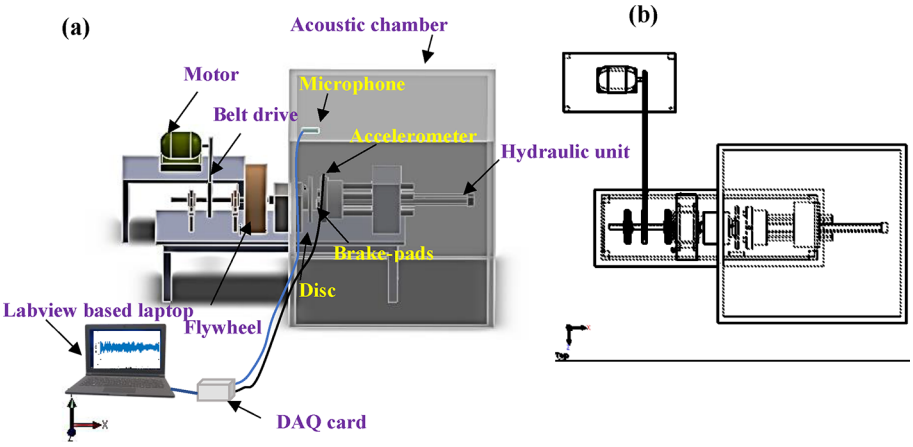

Figure 2. (a) 3D solid work model and (b) top view of the brake noise−vibration test rig.

Table 3. Design of Experiment (DOE) for NV Measurements

braking cycle	pressure (bar)	speed (kmph)	number of brake application	number of NV measurement
bedding	30	80	100	
performance	10, 20, 30	50 and 80	10 each combination	10 each combination
forward/backward	10	20 and −20	10 each combination	10 each combination
drag	10, 20, 30	10 and 20	10 each combination	10 each combination

Table 4. Material Properties Used for FEA Analysis

		brake pad (low metallic)		
property	disc (gray cast iron)	Ref	Zylon fiber	backplate (mild steel)
Young's modulus (GPa)	125	11	11	210
Poisson's ratio	0.25	0.34	0.34	0.3
density (g/cc)	7.16	2.3	2.1	7.85
damping ratio	0.01	0.027	0.040	0.007

using tetrahedral elements. Both models were fine-meshed, and the requisite mesh quality was ensured using quality metrics such as aspect ratio and skewness. In addition, the node convergence study was also done for the disc and brake pad models to check the accuracy of the numerical results, and a model with an optimum element count was chosen. The numbers of finite elements chosen for the disc and the brake pads were 21388 and 3228, respectively.

Table 2 shows the results of the convergence analysis for the initial four modes of the disc and brake pad sample. A mesh with 2−4 mm element sizes was shown as a satisfactory result in

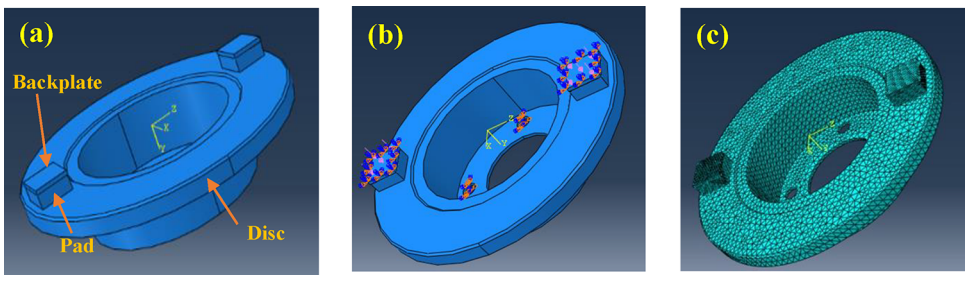

Figure 3. Disc brake system with (a) solid work model, (b) disc−pad boundary conditions, and (c) fine mesh model.

https://doi.org/10.1021/acsomega.2c02313
ACS Omega 2022, 7, 21946−21960

Table 5. Properties of the Developed Brake Pads[43]

property	stds.	units	Ref	AP	AF_1	Z_1	Z_3	Z_6
density		g/cc	2.30	2.16	2.11	2.12	2.14	2.19
water porosity	JIS D 4418	%	8.45	10.28	9.10	9.92	9.94	9.62
oil porosity	JIS D 4418	%	9.81	11.8	10.23	10.64	11.58	10.43
hardness	ASTM D 785	HRR	90.9	93.7	91.8	95.3	92.1	96.6
compressibility	ISO 6310	μm	57	76	72	81	87	74

relation to experimental and numerical accuracy. The corresponding numbers of nodes and elements for the different element sizes are also studied and reported in Table 2. In addition, the percentage change in the natural frequencies for the initial four modes is shown in Table 2. Finally, the 2 mm element size was chosen as the natural frequencies were close to the experimental natural frequencies within an error of 2%.

2.4. Brake Noise and Vibration Evaluation. The developed brake pads were characterized for noise and vibration (NV) performance on the in-house-developed NV test rig (the test rig specifications are detailed in ref 30 as shown in Figure 2).

The brake pad samples (size : 25 mm × 25 mm) were cut from the developed pads and fixed in the pad holder slots as shown. In addition, the brake disc (material, gray cast iron) was fixed opposite to the pads. The hydraulic pressure system was used to perform the braking operation. The sound pressure and vibration signals were recorded using a microphone (model: PCB make model 377C13) and accelerometer (model: PCB make model 352C03) during braking operations. The microphone position was set as per the SAE J 2521 test standard, 50 cm above and 10 cm offset from the center of the disc. The acquisition of vibration and sound pressure data and subsequent processing were done using an NI DAQ express system using an NI-9234 data card. The sampling rate of 25600/s was chosen for the NV tests. Table 3 shows the design of experiments (DOE) for brake NV performance evaluation. Before starting the actual test, a bedding operation was performed to get the conformal contact for all pads. All the tests were performed under the same test conditions (i.e., background noise level of <45 dBA, relative humidity of 50 ± 10% RH, and temperature of 30 ± 2 °C) in the laboratory. The fresh brake pads and disc were used for each test. Brake NV signals were recorded for 10 braking applications in each cycle and used for the NV analysis. The octave band analysis of the acquired acoustic pressure time-domain vibration of acceleration data was carried out in an in-house-developed MATLAB code.

2.5. Brake Squeal Prophecy Model. *2.5.1. Modeling of the Disc−Brake Pad System.* For the brake pad−disc assembly, it was decided to investigate the eigenvalue analysis in ABAQUS. A solid model of disc and pads was prepared as per the dimensions of the discs and pad samples as shown in Figure 3. Later, this solid model was imported into ABAQUS/CAE and was fine-meshed. The mesh quality was confirmed using elemental failure criteria with right values of shape factor and aspect ratio used, and analysis errors and warning were checked and found to be 0%.

The equation of motion of the disc brake unit can be written as follows:[3]

$$[M_f]\{\ddot{x}\} + [C_f]\{\dot{x}\} + [K_f]\{x\} = 0 \quad (1)$$

where $\{x\}$ is a nodal displacement vector, and $[M_f]$, $[C_f]$, and $[K_f]$ are the mass, damping, and stiffness matrices of the system, respectively.

The above matrices are asymmetric due to friction. The greater the asymmetry, the more easy the possibility of friction-induced vibration of the disc brake system.[48]

In the current work, the complex eigenvalue analysis (CEA) method was used to solve the equation of motion of the disc−pad system. The CEA helps in finding all unstable eigenvalues and corresponding vibration modes under the condition of linearized nonlinearities, which are close to steady sliding states. In the CEA, the eigenvalue equation can be represented as follows:

$$([M_f]\lambda^2 + [C_f]\lambda + [K_f])\phi = 0 \quad (2)$$

where λ is the eigenvalue and ϕ is the corresponding eigenvector. Additionally, the general solution can be found using the subspace iteration technique, which is as follows:

$$x(t) = \sum_{i=1}^{n} \phi_i\{\exp(\alpha_i + j\omega_i)t\} \quad (3)$$

where "t" is the time and α_i is the real part and ω_i is the imaginary part for the ith eigenvalue. If the real part of the eigenvalue (α) is a positive value (i.e., $\alpha > 0$), then it indicates an unstable vibration of the brake system. The brake system thus vibrates with a large amplitude of vibration. Generally, the effective damping ratio (ζ_E) is used to quantify the intensity of unstable vibration, which is defined as,[10]

$$\zeta_E = \frac{-2(\text{real part }(\lambda))}{(\text{imaginary part }(\lambda))} \quad (4)$$

The unstable vibrations can occur if the effective damping ratio is negative (i.e., $\zeta_E < 0$). The smaller the ζ_E value, the more the corresponding squealing vibrations are. The effective damping ratio (ζ_E) can be obtained from the CEA.

2.5.2. Model Constraints and Parameters. Figure 3 shows the disc brake system consisting of brake pads and a disc. For carrying out the eigenvalue analysis, the FE model of pads and the disc is created. In the fine mesh model, there are a total of 49382 nodes and 46062 elements (types: disc, C3D10; pad and backplate, C3D8R). All the nodes of the central holes of the disc were fixed in all directions (i.e., x, y, and z). The brake disc and pads are the friction surface pairs. The pads were connected to backplates using tie-type constraints of ABAQUS. The tangential behavior with the penalty method was used as a contact property for the disc−pad pair. The friction coefficient was considered as a constant value during the sliding for the selected operating pressure and speed condition. The material properties of brake discs, pads, and backplates are enlisted in Table 4. The value of the positive real part has a strong correlation with the friction-induced vibrations. Thus, the eigenvalue with the positive real part indicates an unstable frequency of vibration that in turn reflects into a squeal frequency.

https://doi.org/10.1021/acsomega.2c02313
ACS Omega 2022, 7, 21946−21960

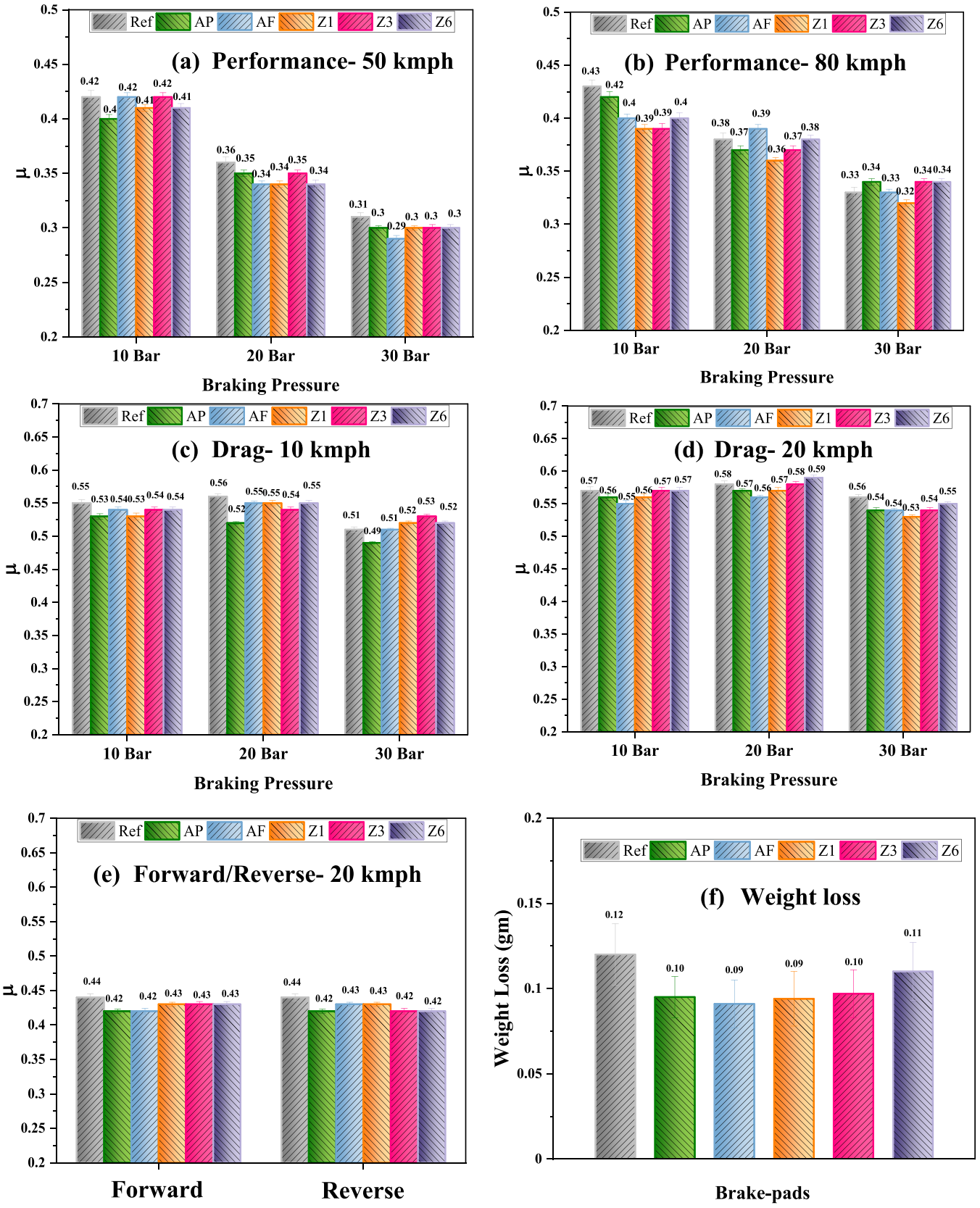

Figure 4. (a−e) Average coefficient of friction in braking cycles and (f) weight loss of brake pads.

3. RESULTS AND DISCUSSION

3.1. Characterizations of Brake Pads. Table 5 enlists the physical and mechanical properties of the developed pads.[43] The density was the highest for the reference pad due to the high amount of higher density space filler (i.e., barite). However, aramid/Zylon fiber-based pads showed more or less similar density values except the Z_6 pad. The reference pad showed the

https://doi.org/10.1021/acsomega.2c02313
ACS Omega 2022, 7, 21946−21960

Table 6. Natural Frequencies and Mode Shapes for the Disc and Brake Pad Samples

Mode no.	Disc		Brake pad sample (1 × 1 inch)			
			Reference pad		Aramid/Zylon fiber pad	
	Natural frequency (Hz)	Mode shape	Natural frequency (Hz)	Mode shape	Natural frequency (Hz)	Mode shape
1	1726	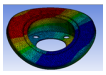	9754	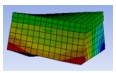	10356	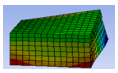
2	3326	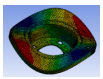	12095	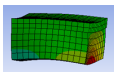	12307	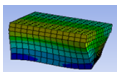
3	6945	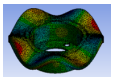	13072	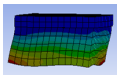	13685	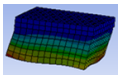
4	9299	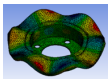	13929	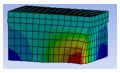	14714	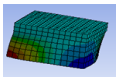
5	11953	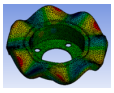	15153	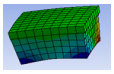	15922	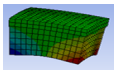
6	14855	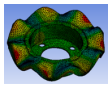	-	-	-	-

lowest porosity and compressibility, while higher compressibility was found for aramid fiber- and Zylon fiber-based pads. Slightly higher compressibility was observed for Z_3 and Z_1 pads compared to aramid fiber-based pads. The marginal difference in hardness was observed for all pads. Porosity, compressibility, and hardness can affect brake NV performance.[44]

3.2. Friction and Wear Studies. Figure 4a−e shows the friction and wear results for the tested pads during the NV cycles.

The average coefficient of friction (μ) values of 10 brakes with standard deviations are reported for all braking cycles. It was observed that the average μ was more or less similar for all pads except a few cases. The aramid short fibers showed slightly higher μ compared to aramid pulp-based pads. However, with the increasing size of Zylon fibers, a marginal difference was observed in all cycles. Overall, the reference pad showed slightly more fluctuation in μ compared to aramid fiber- and Zylon fiber-based pads. Figure 4f shows the weight loss of the brake pads after the competition of test. The wear resistance was compared to all other types of pads. Aramid and Zylon short fibers proved to be the best, while the reference pad proved to be the worst in wear resistance. Wear was increased slightly with the increase in the size of fibers.

3.3. Modeling of the Brake Pad and Brake Disc. Using the FE model for pads and discs, eigenvalue analysis has been carried out, and Table 6 details the natural frequencies and mode shapes for the brake disc and brake pad samples.

Corresponding to the disc natural frequencies, the reference pad frequencies such as mode 2 (12095 Hz) and mode 5 (15153 Hz) are very close to the natural modes of the disc (modes 5 and 6). The same is observed in mode 4 of the aramid/Zylon fiber-based pad. The closeness leads to a ready mode coupling and stronger vibration levels. However, the overall modal damping can play an important role in the unstable vibration.

3.3.1. Experimental Modal Analysis. Figure 5 shows the experimental FRF based on measurement data for the developed brake pads. The FRF shows the variation of the ratio of the amplitude (acceleration, m/s^2) and applied force (N) with frequency (Hz). The blue curve shows the FRF for the pads. The circle fit method was used to find and locate the modal frequencies (for the natural modes). The blue curve displays the FRF plots based on the measured data, while the red curve represents the curve-fitted FRF based on the circle fit method using the resonances picked up and chosen from the measured FRF plot.[45] The initial four modes of vibrations for each brake pad were chosen, and the corresponding identified natural frequencies and damping ratios are reported in Table 7.

Overall, it may be noted from the amplitudes of the peaks in the FRF that due to the inclusion of aramid and Zylon fibers, damping improved significantly, and natural frequencies were reduced for most cases. However, the short fibers (1 mm) of aramid and Zylon proved to be the best for the average damping ratio, while the reference proved to be the worst.

Figure 6 shows the comparison of the natural frequencies obtained from experimental and numerical (FEA) methods with corresponding mode shapes (B, bending; T, twisting) for reference brake pads. The natural frequencies of pads using experimental and numerical methods were observed to be more or less similar with a marginal difference (<5%) except the second mode. Additionally, a slight difference (4−8%) in the natural frequency of the disc rotor was observed for experimental and numerical methods. Overall, it is noted that the numerical FE model of the brake components is reasonably accurate.

https://doi.org/10.1021/acsomega.2c02313
ACS Omega 2022, 7, 21946−21960

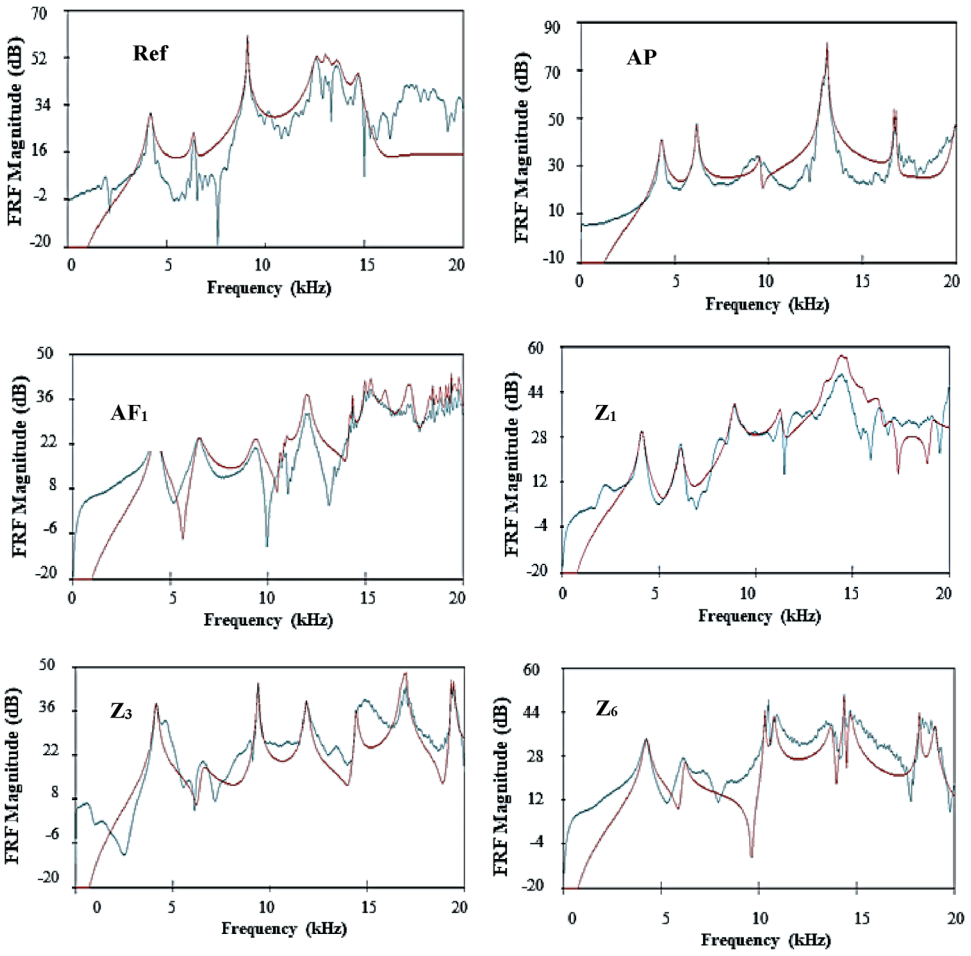

Figure 5. FRF plots for the developed brake pads (blue: measured; red: curve-fitted).

Table 7. Experimental Natural Frequencies and Damping Ratios of Pads[a]

	brake pad											
	Ref		AP		AF_1		Z_1		Z_3		Z_6	
mode	ω (Hz)	ζ	ω (Hz)	ζ	ω (Hz)	ζ	ω (Hz)	ζ	ω (Hz)	ζ	ω (Hz)	ζ
1	4175	0.045	4175	0.048	4275	0.065	4125	0.051	4150	0.035	4225	0.047
2	6375	0.023	6250	0.035	6600	0.024	6125	0.048	6525	0.055	6100	0.038
3	9350	0.010	7850	0.019	9375	0.055	8975	0.036	9400	0.024	8850	0.029
4	12575	0.029	12300	0.031	10625	0.014	11350	0.023	11900	0.021	12,625	0.036
avg. damping	0.027		0.033		0.040		0.040		0.034		0.038	

[a]Here, ω is the natural frequency (Hz), and ζ is the damping ratio.

3.4. Brake Noise and Vibration Performance. The brake pads were assessed for experimental NV performance for four braking cycles (viz., performance, forward, backward, and drag) under various pressure and speed conditions. The pad−disc touch times of 1 s for the performance cycle, half-second for forward/backward cycles, and 4 s for the drag cycle were kept fixed during the braking operations. Figures 7 and 8 highlight the time-domain and fast Fourier transform (FFT) vibration (g) spectra for braking and no-braking conditions. The acquisition of braking NV signals was started before the engagement of brake pads with the disc and stopped after disengagement for all the brake cycles. The analysis of braking signals was done for the actual braking time, as shown in the time domain in Figures 7c and 8c. Figure 7a,b shows the time domain and FFT plot (entire frequency range: 0−12,800 Hz) for the no-braking condition (80 kmph). As expected, the amplitude of vibration increased due to the braking action compared to the no-braking condition. The frequency spectra (Figure 7b) show the presence of some small amplitude (<0.01 g) vibrational frequencies (49 and 61 Hz), which could be related to the rotational motion of the disc or structural vibration. Figure 7c,d shows the time domain and FFT plot for the braking action (reference pad). The FFT plot (Figure 7d) clearly indicates that the vibration amplitude drastically increased due to friction-induced vibration between tribo-couples (pad−disc). Due to the braking action, new vibrational frequencies (47, 193, 383, and 580 Hz and some high-frequency vibrations) appeared, which are highlighted in Figure 7d. The higher frequency vibrations (10−12 kHz) were observed due to structural resonances. FFT plots of low-frequency regions for all pads are shown in Figure 7d,f−j.

https://doi.org/10.1021/acsomega.2c02313
ACS Omega 2022, 7, 21946−21960

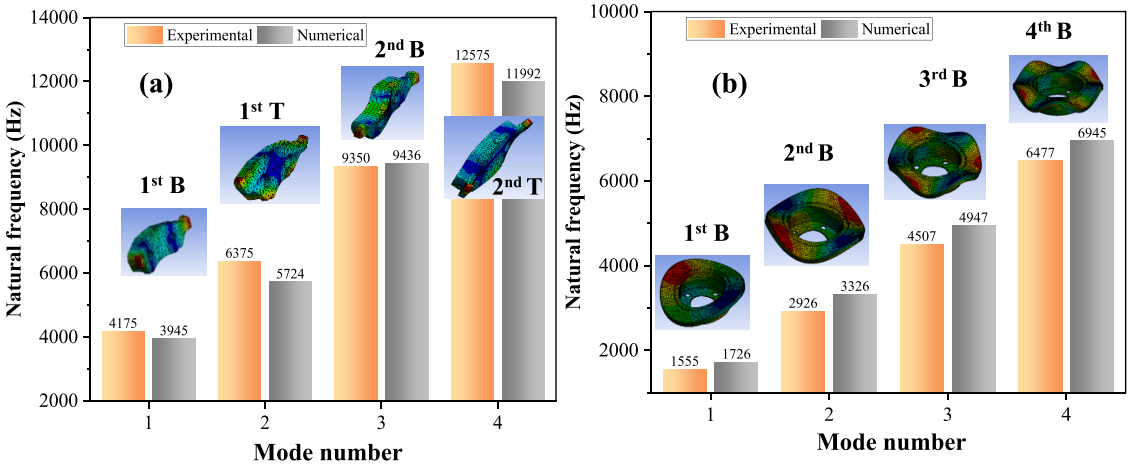

Figure 6. Experimental and numerical natural frequency results for (a) brake pads and (b) disc rotor with corresponding mode shapes.

As discussed later, the brake noise spectra were dominated by mainly the low-frequency components (<500 Hz).

The time- and frequency-domain vibration data for the drag cycle (speed, 10 kmph; pressure, 10 bar condition) are shown in Figure 8. The braking action led to an increase in vibration level significantly compared to the no-braking condition, as shown in Figure 8a,c,e. The reference pad showed more unsteady and higher vibrations compared to aramid/Zylon fiber-based pads due to their lower damping, porosity, and compressibility values. Brake vibrations are directly proportional to the damping property of materials.[29,30,44,45] Tables 5 and 6 show that the porosity, compressibility, and damping values were lower for reference pads than aramid/Zylon fiber-based pads. The damping performance order of brake pads was as follows: AF_1 (0.40) = Z_1 (0.40) > Z_6 (0.38) > Z_3 (0.34) > AP (0.33) > Ref (0.27).

In addition, there was a more or less similar trend observed in the vibration amplitude for other pads, as shown in Figure 8f−j.

Overall, the higher values of compressibility, porosity, and damping resulted in attenuation of the vibration amplitude during the braking action for all the cycles, which finally influenced better noise performance, which will be discussed in the later section.

3.4.1. Root Mean Square (RMS) Vibration. The noise and vibration measurements were repeated 10 times for all the brake pads in each braking cycle, and the measured data were averaged out. The noise and vibration readings are therefore an average value of 10 readings. Figure 9a−e shows the average RMS vibration during braking under different brake conditions for all the pads. The average RMS vibration (in g) values were calculated for the entire frequency range (0−12800 Hz).

It was observed that the RMS vibration increased for the same pressure conditions with an increase in speed. However, there was a slight drop in the RMS vibration with an increase in pressure for the same speed condition. Overall, the aramid/Zylon fiber-based brake pads showed lower average RMS vibrations in all the brake cycles compared to the reference pad. Figure 9f shows the overall improvement in the RMS vibration (%) for aramid/Zylon fiber-based pads compared to the reference pad considering all the braking cycles. The Z_6 pad proved to be the best with a maximum improvement (26.3%) in average RMS vibration compared to the reference pad. Additionally, the other two pads, short aramid (AF_1) and Zylon (Z_1), showed more or less similar improvement (21−22%) in average RMS vibration.

3.4.2. Brake Noise Performance. Figure 10a−e shows brake noise level (dBA) results during the braking action for various test conditions. According to the SAE J 2521 test schedule, the background noise level was maintained below 60 dBA inside the acoustic chamber for all the speeds in the no-braking conditions. It was observed that the noise level increased with an increase in speed for the same pressure condition. The brake noise level was raised as the pressure increased for all pads except a few cases in the performance cycles. The reference pad showed the highest noise level compared to all pads. The brake noise level dropped (drag: 1−1.5 dBA ± 0.3−0.4 dBA; performance: 1−1.5 dBA ± 0.5−0.7 dBA; forward/backward: 2−2.5 dBA ± 1−1.5 dBA) for aramid/Zylon fiber-based pads compared to the reference pad. Overall, the reduction in brake noise (dBA) due to aramid/Zylon fibers in the pad is shown in Figure 10f. The AF_1 and Z_3 pads showed a maximum reduction in the overall noise level (1.5 dBA). Additionally, AP, Z_1, and Z_6 pads showed an almost similar reduction in the overall noise level (1.2 dBA). Overall, the short aramid fiber (AF_1)- and Zylon fiber (Z_3)-based pads proved to be the best in noise performance among all pads.

3.5. Brake Squeal Quantification. *3.5.1. Experimental Analysis.* Figure 11 shows the time-domain and vibration (g) spectra for reference and Zylon fiber-based pads in the forward brake cycle. Brake squeal was observed under low-speed, low-pressure test conditions for the reference pad only in the forward cycle. No squeal was observed for high-speed and high-pressure (>10 bar) conditions. However, in the forward cycle, friction was observed in the range of 0.42−0.44.

The high-frequency brake squeal was observed at a frequency of 9381 Hz for the reference pad, and the corresponding time-domain and vibration (g) spectra are highlighted in Figure 11a,b. It may be noted that the third mode of the brake pad−disc assembly is found to be 9350 Hz (Table 7). The main reasons of squeal in the case of the reference pad (i.e., without aramid/Zylon fibers) are higher density and lower damping of pad material in addition to friction. All the aramid fiber- and Zylon fiber-based pads showed no squeal tendency for all selected test conditions due to their lower density and higher damping of pad material, although friction was almost in a similar range as that of the reference pad. Figure 11c,d shows the time domain and FFT plot of vibration for the Zylon fiber-based pads. A similar trend in vibration spectra was observed for other Zylon fiber- and

https://doi.org/10.1021/acsomega.2c02313
ACS Omega 2022, 7, 21946−21960

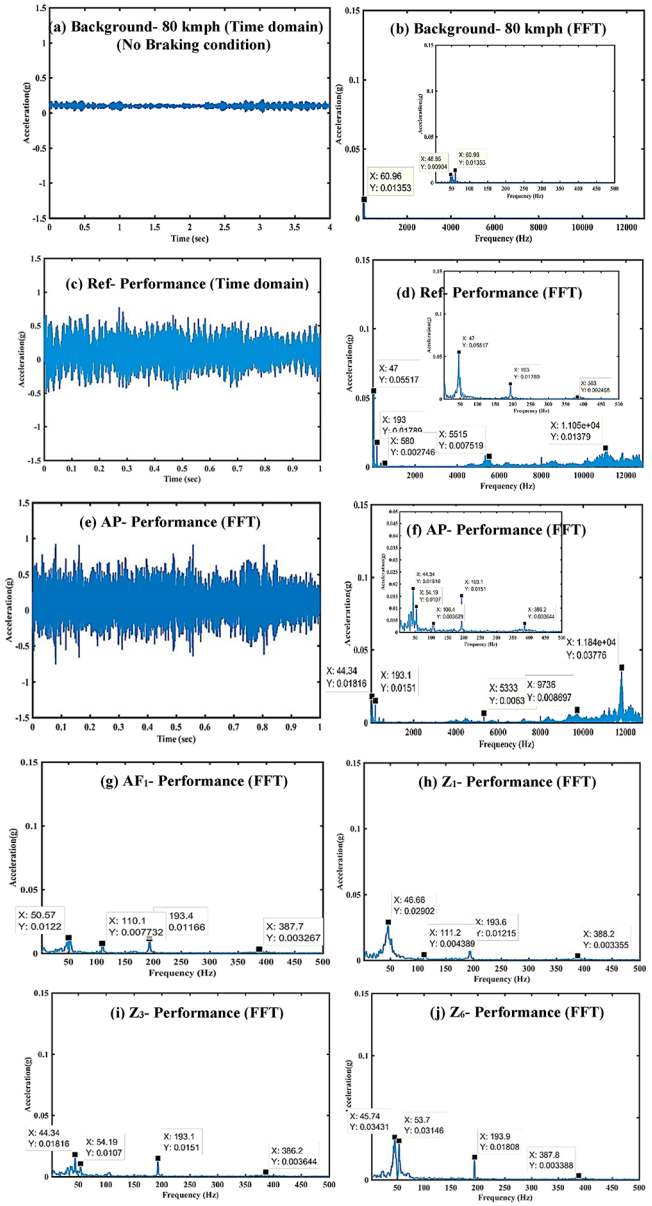

Figure 7. (a, c, e) Time-domain and (b, d, f–j) FFT spectra of vibration (g) without (background) and with braking conditions (performance cycle, 80 kmph, 10 bar).

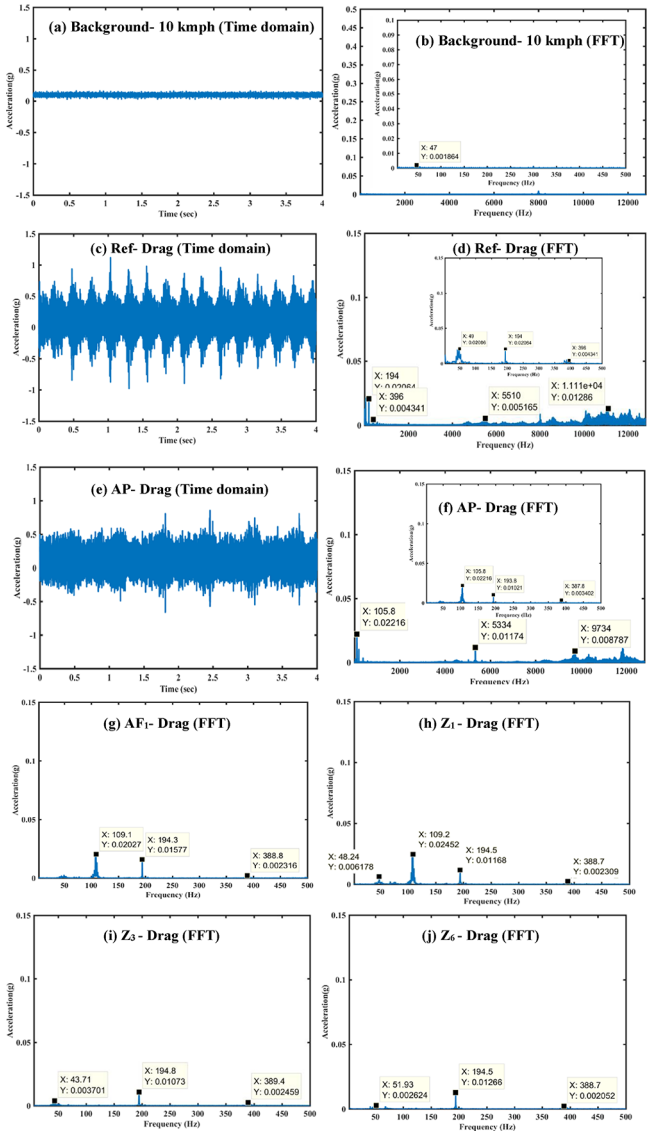

Figure 8. (a, c, e) Time-domain vibration response and (b, d, f–j) corresponding frequency spectra with and without braking conditions (drag cycle, 10 kmph, 10 bar).

aramid fiber-based pads. The brake vibration amplitude was lower and without any squeal frequency in aramid fiber- and Zylon fiber-based pads compared to the reference pad (without aramid/Zylon fibers). Figure 11d shows no squeal frequency in the brake vibration spectra.

3.5.2. Numerical Analysis. Complex eigenvalue analysis (CEA) on a mechanical system helps one to understand the nature of the eigenvalues of the system. The real part of the complex eigenvalue thus obtained gives information on the stability of the vibratory system. It is used to find the unstable modes of vibration, and the corresponding mode shapes can be extracted. It is common to model the vibratory system using the finite element approach by discretizing the continuum into several discrete finite elements. This discretized model and subsequent numerical approach to find the set of complex eigenvalues with their real and imaginary parts help identify the rate of growth and unstable frequencies of the system.[10,46] In the current study, CEA is performed to predict the possible unstable eigenfrequencies of the brake pad–disc assembly between 0 and 16 kHz for the forward cycle (speed, 20 kmph; pressure, 10 bar condition) for the brake squeal prophecy of the developed pads.

In the CEA, the actual density, damping, and friction properties were considered, while the elastic modulus (E) and Poisson's ratio were assumed to be constant for all pads. Table 8 shows the material properties of brake system components. Figure 12 shows the mode shapes of the brake pad–disc assembly obtained through the FE simulation. The results in Table 9 show three dominant unstable frequencies (i.e., 9226, 11,809, and 14,593 Hz) for the reference pad and corresponding absolute values of the real part of the eigenvalue (i.e., 14.2, 353.7, and 1352) and effective damping ratio (i.e., −0.003, −0.061, and −0.185). The simulated natural frequency of the reference brake pad (9226 Hz) matches close to the experimentally observed natural frequency of 9350 Hz (Table 5). The additional one unstable vibration frequency close to 11800 Hz (Figure 12b,e) is observed in numerical analysis (CEA) in contrast to experimental analysis for the selected frequency range (0–

https://doi.org/10.1021/acsomega.2c02313
ACS Omega 2022, 7, 21946−21960

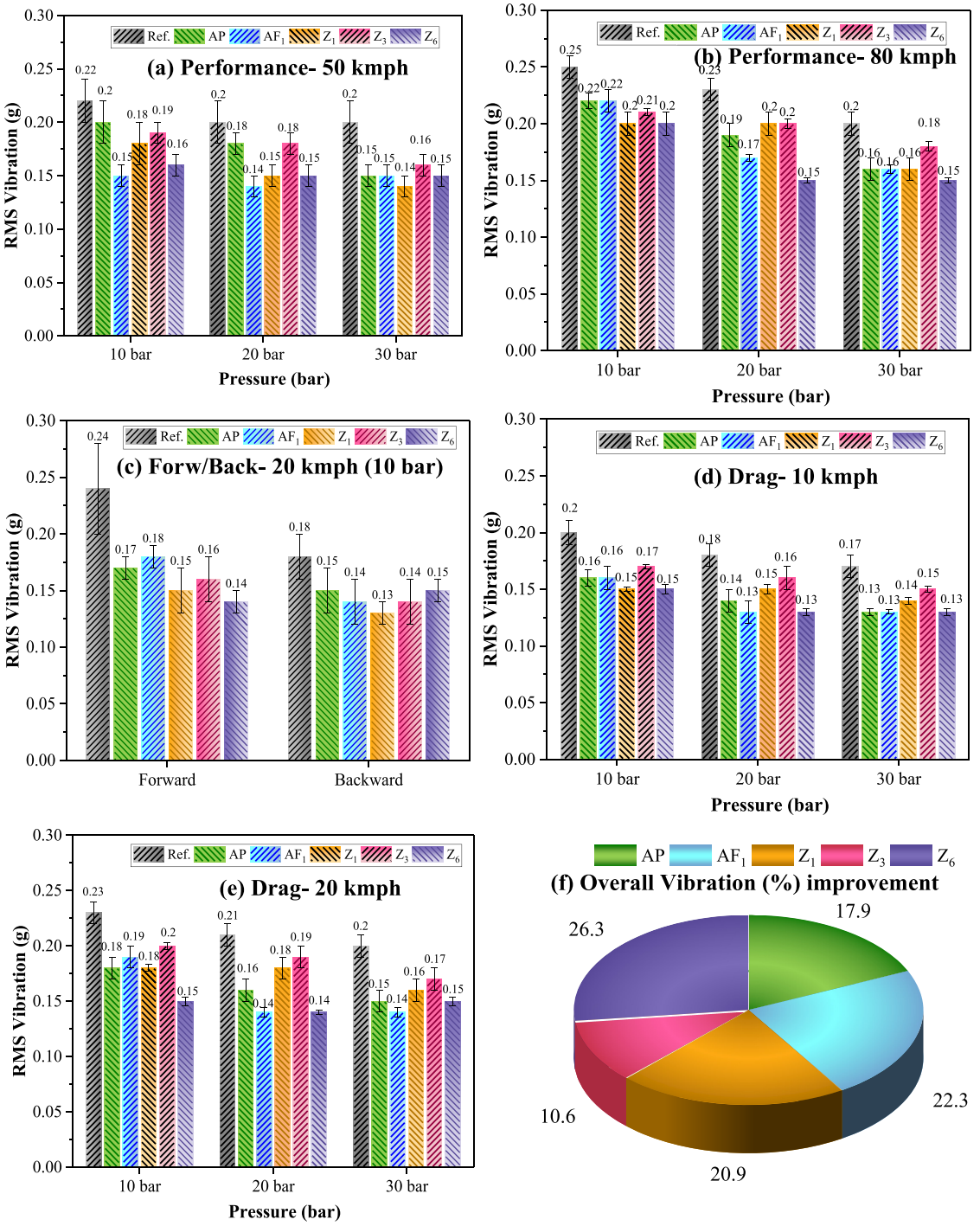

Figure 9. (a−e) Average RMS vibration (g) during braking conditions for different brake pads. (f) Overall improvement in RMS vibration (%) relative to the reference pad considering all braking cycles.

12800 Hz). The brake pad and disc may be coupled at higher frequencies due to friction when the pad−disc natural frequencies come closer. If modal frequencies of the pad−disc pair are close, then modal coupling occurs and generates the brake squeal. In the current study, the modal frequencies of the disc (9299 Hz) and reference pad sample (9754 Hz) are closer to the observed squeal frequency. However, the first natural frequency of aramid fiber- and Zylon fiber-based pads occurred around 10356 Hz, which was far from the disc modal frequency (9299 Hz). In addition to this, the next modal frequencies for the disc and pads are closer to a higher frequency range beyond 12000 Hz and may not be readily excited. The probability of squeal noise generation can be reduced by reinforcing high damping aramid/Zylon fibers in the pad and ensuring the adequate difference in the modal frequencies of the brake pad and disc.

In addition to the above studies, the effect of damping was studied for reference and aramid/Zylon fiber-based pads, as shown in Figure 13. The results revealed that with an increase in the damping of the pad, the effective damping ratio (i.e., brake squeal intensity) decreased slightly for both pads. Overall, it was found that the density of the brake pad plays a vital role in

https://doi.org/10.1021/acsomega.2c02313
ACS Omega 2022, 7, 21946−21960

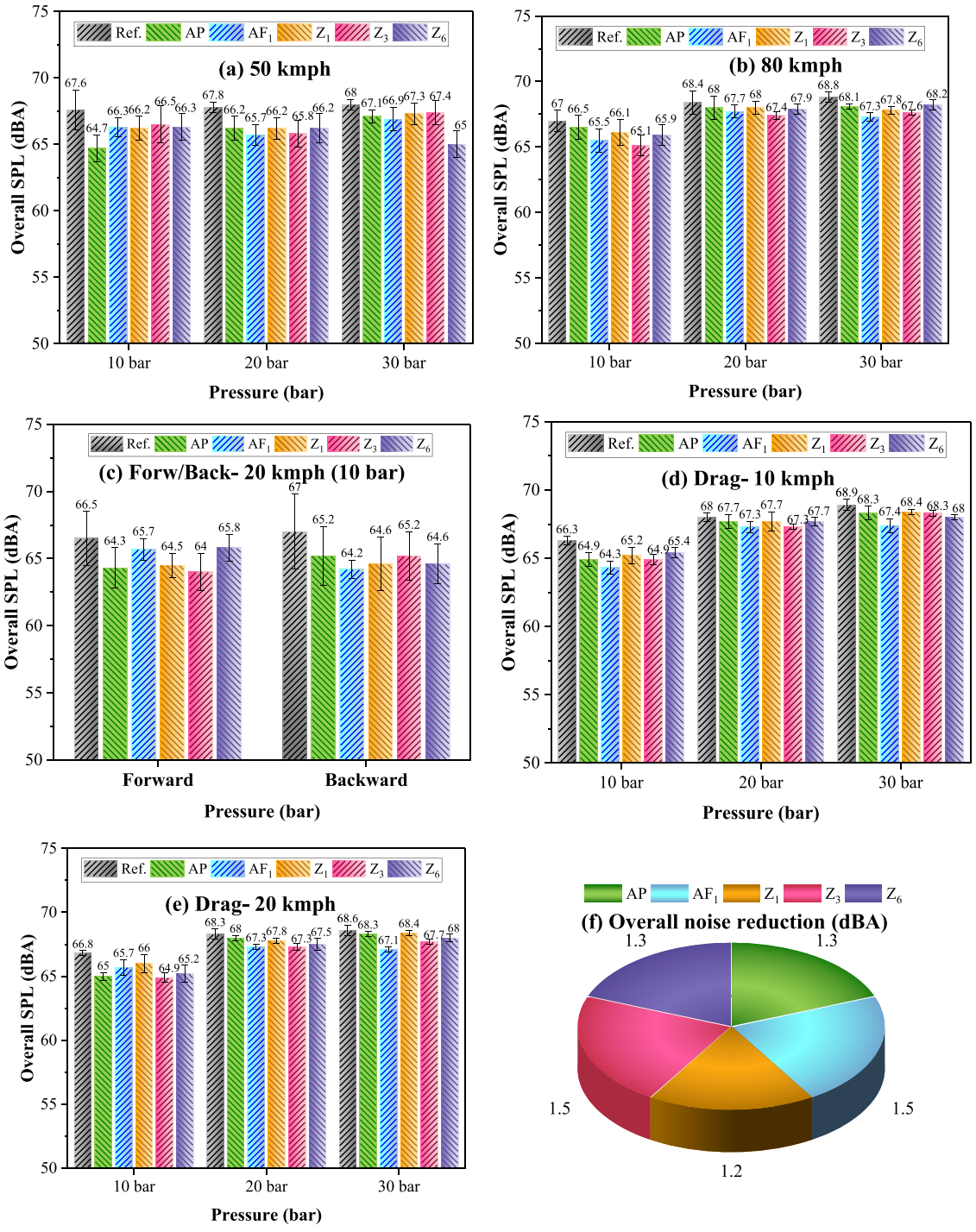

Figure 10. (a–e) Overall sound pressure level (dBA) during braking conditions for different brake pads. (f) Overall reduction in SPL (dBA) relative to the reference pad considering all braking cycles.

addition to the damping in reducing the brake squeal propensity.[49]

Generally, the magnitude of the real part of the eigenvalue shows the brake squeal propensity to a certain degree. However, there are various unstable frequencies that show the squeal propensity. Thus, to quantify the squeal propensity for these three types (Ref, aramid, and Zylon fibers) of pads, the tendency of instability (TOI) is calculated using the given formula.[47]

$$\mathrm{TOI} = \sum_{j=1}^{n} \left(\frac{\alpha_j}{\omega_j} \times 1000 \right), \ \alpha_j > 0 \tag{5}$$

where α_j and ω_j are the real and imaginary parts of the jth eigenvalue, and n is the total number of positive eigenvalues.

Figure 14 shows the TOI of three types of brake pads. The squeal propensity is larger for higher TOI. While the reference pad shows the TOI of 127.3, the aramid fiber-based pad showed the lowest (100.3) TOI, followed by Zylon fiber-based pads with more or less similar values (102.9). The TOI was mainly

https://doi.org/10.1021/acsomega.2c02313
ACS Omega 2022, 7, 21946−21960

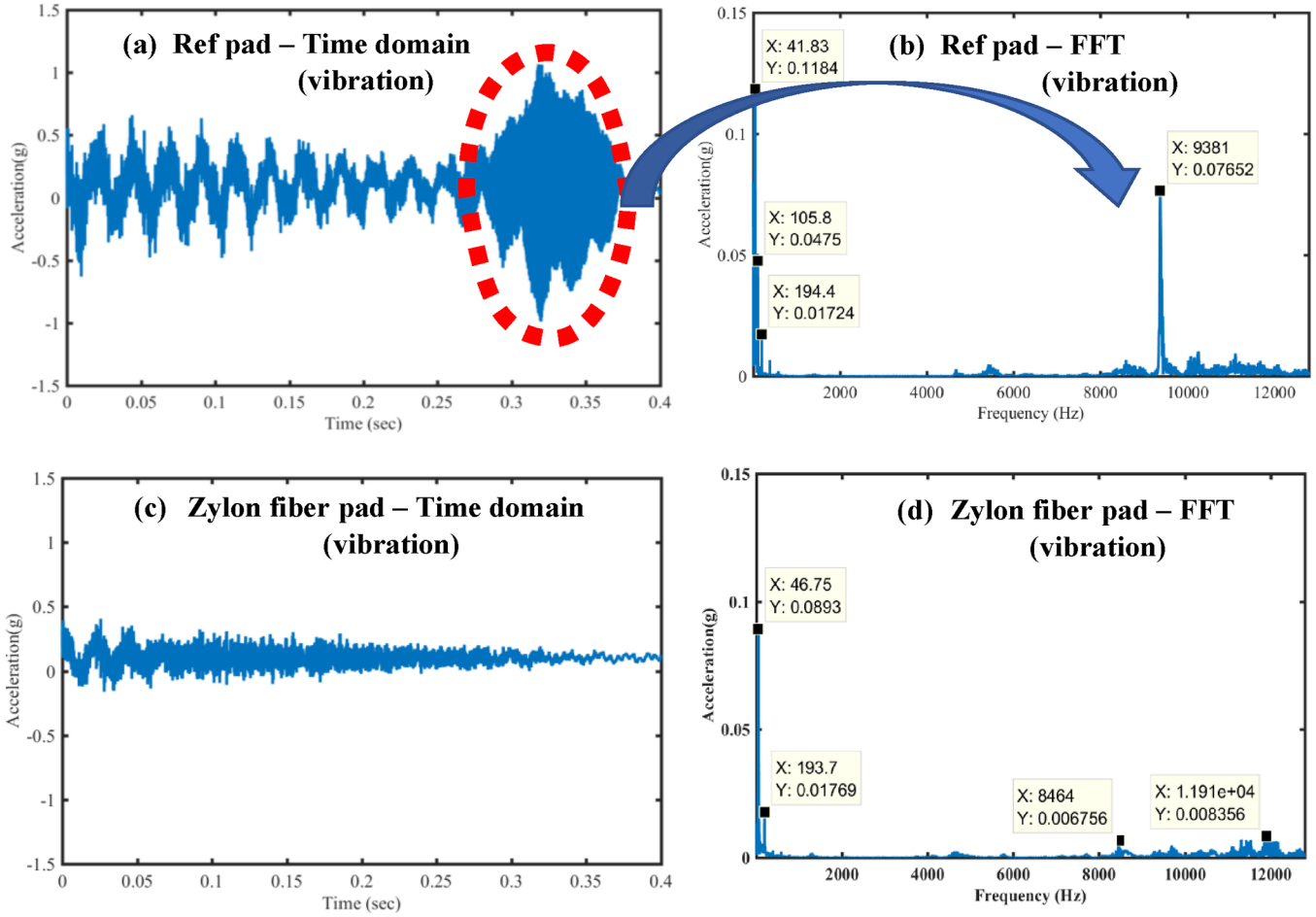

Figure 11. Time-domain and FFT spectra of brake vibration (g) for (a, b) reference and (c, d) Zylon fiber-based pads in a forward cycle.

Table 8. Material Properties of Brake System Components

			brake pad	
property	disc	backplate	Ref	Zylon fiber
Young's modulus (GPa)	125	210	11	11
Poisson's ratio	0.23	0.3	0.34	0.34
density (g/cc)	7.16	7.85	2.3	2.1
damping ratio	0.01	0.007	0.027	0.04

controlled by enhancing the damping of brake pads as shown in Table 7. The reference brake pad comprises barite ($BaSO_4$) having a higher density (ϱ = 4.4 g/cc) instead of lighter ingredients (ϱ = 1.44−1.54 g/cc) such as aramid and Zylon fibers, thus decreasing the density of brake pads. The inclusion of fibers leads to higher porosity and, hence, compressibility compared to particulate ingredients, which further leads to enhanced damping.[43] Overall, the improvement in the squeal propensity is 21.2 and 19.2% for aramid fiber- and Zylon fiber-based pads relative to the reference pad, respectively. Hence, the

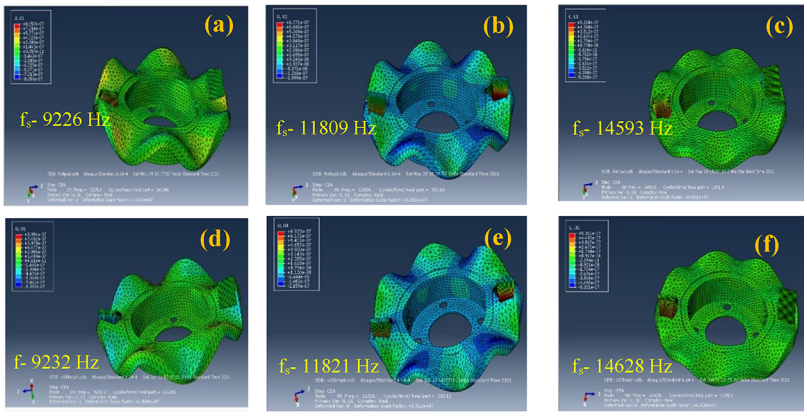

Figure 12. Mode of vibration for (a−c) reference pad-unstable modes, (d) Zylon fiber pad-stable mode (no squeal event), and (e, f) Zylon fiber pad-unstable modes (f_s, squeal frequency).

https://doi.org/10.1021/acsomega.2c02313
ACS Omega 2022, 7, 21946−21960

Table 9. Real Parts of Complex Eigenvalue and Effective Damping Ratio for Squeal Frequencies

reference pad			Zylon fiber pad		
squeal frequency (Hz)	eigenvalue (real part)	effective damping ratio (ζ_E)	squeal frequency (Hz)	eigenvalue (real part)	effective damping ratio (ζ_E)
mode 29: 9226	14.2	−0.003	mode 29: 9232	−16.2	0.004
mode 39: 11809	353.7	−0.060	mode 39: 11821	295.1	−0.050
mode 50: 14593	1352	−0.185	mode 50: 14628	1165.1	−0.159

inclusion of aramid or Zylon fibers is an effective method to minimize the squeal propensity through damping enhancement.

In addition, the wear mechanism is already explained in our earlier tribological article,[43] and this article was a part of the noise−vibration study. The reference pad showed more unstable secondary plateaus and more wear debris on the surface. More secondary plateaus support higher wear of the pad.[51] The friction materials with large contact plateaus produced squeal noise due to the high impact energy transferred to the brake assembly. In contrast, the specimens with small plateaus produced chatter without squeal noise. The control of contact plateaus could be the key to reduced friction-induced vibrations.[11] In the earlier tribological study, similar mechanisms (more contact plateaus) were observed without aramid/Zylon fiber-based pads.[43]

4. CONCLUSIONS

In the present work, various types of aramid/Zylon fiber-based brake pads were evaluated for noise and vibration characteristics on the developed brake noise−vibration test rig. In addition, the analysis of brake squeal frequencies was done using both methods (i.e., experimental and numerical). The following are the salient conclusions that were drawn.

The inclusion of aramid/Zylon fibers in the pads aided in decreasing the density and increasing the porosity, compressibility, and damping properties of the brake pads compared to the reference pad.

Experimental results of the noise−vibration (NV) test rig showed that damping, compressibility, and density control the intensity of noise and vibration. It was found that both low- and high-frequency noise and vibration can be suppressed using high damping aramid and novel Zylon fibers in the pads without affecting the friction performance.

Overall reduction in the brake noise (1.2−1.5 dBA) and improvement in vibration (20−25%) were observed for aramid fiber- and Zylon fiber-based pads relative to the reference pad.

Complex eigenvalue analysis of the brake system showed that brake squeal was mainly influenced by the damping and density of the pad materials.

Aramid/Zylon fiber-based brake pads can effectively suppress the instability of the brake system and reduce the brake squeal propensity.

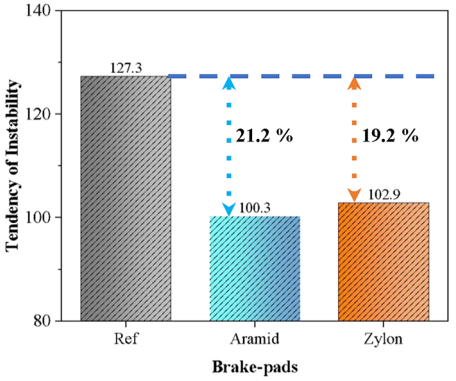

Figure 14. Tendency of instability (TOI) of three types of pads.

AUTHOR INFORMATION

Corresponding Author

Jayashree Bijwe − *Centre for Automotive Research and Tribology (CART), Indian Institute of Technology Delhi, New Delhi 110016, India;* orcid.org/0000-0003-0695-2355; Email: jbijwe@gmail.com

Authors

Navnath Kalel − *Centre for Automotive Research and Tribology (CART), Indian Institute of Technology Delhi, New Delhi 110016, India*

Bhaskaranand Bhatt − *Centre for Automotive Research and Tribology (CART), Indian Institute of Technology Delhi, New Delhi 110016, India*

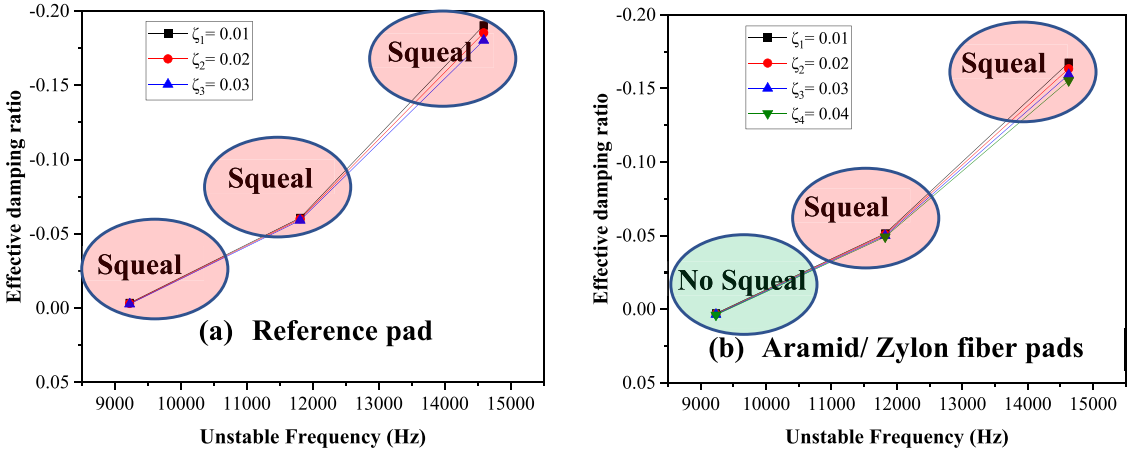

Figure 13. Effect of pad damping on squeal for (a) the reference pad and (b) aramid/Zylon pad.

https://doi.org/10.1021/acsomega.2c02313
ACS Omega 2022, 7, 21946−21960

Ashish Darpe − *Department of Mechanical Engineering, Indian Institute of Technology Delhi, New Delhi 110016, India*

Complete contact information is available at: https://pubs.acs.org/10.1021/acsomega.2c02313

Notes

The authors declare no competing financial interest.

■ ACKNOWLEDGMENTS

The authors would like to thank Mr. Raj Khanolkar, Tech. Director of MASU Brakes Pvt. Ltd., India, for assisting in the hardness and compressibility tests of the brake pads. The authors are thankful to Mr. Pravin Jain, Director Super Circle Auto Limited, Delhi, and Mr. Sudhir Dixit (Corporate Business Head, Super Circle Auto Limited, Delhi) for providing backplates for the brake pads.

■ REFERENCES

(1) Akay, A. Acoustics of friction. *J. Acoust. Soc. Am.* **2002**, *111*, 1525−1548.
(2) Kinkaid, N. M.; O'Reilly, O. M.; Papadopoulos, P. Automotive disc brake squeal. *J. Sound Vib.* **2003**, *267*, 105−166.
(3) Ouyang, H.; Nack, W.; Yuan, Y.; Chen, F. Numerical analysis of automotive disc brake squeal: a review. *Int. J. Veh. Noise Vib.* **2005**, *1*, 207−231.
(4) Dai, Y.; Lim, T. Suppression of brake squeal noise applying finite element brake and pad model enhanced by spectral-based assurance criteria. *Appl. Acoust.* **2008**, *69*, 196−214.
(5) Tang, B.; Mo, J.-L.; Wu, Y.; Quan, X.; Zhu, M. H.; Zhou, Z. R. Effect of the friction block shape of railway brakes on the vibration and noise under dry and wet conditions. *Tribol. Trans.* **2019**, *62*, 262−273.
(6) Poletto, J. C.; Neis, P. D.; Ferreira, N. F.; Masotti, D.; Matozo, L. T. An experimental analysis of the methods for brake squeal quantification. *Appl. Acoust.* **2017**, *122*, 107−112.
(7) Kchaou, M.; Lazim, A.; Hamid, M.; Bakar, A. Experimental studies of friction induced brake squeal: influence of environmental sand particles in the interface brake pad-disc. *Tribol. Int.* **2017**, *110*, 307−317.
(8) Renault, A.; Massa, F.; Lallemand, B.; Tison, T. Experimental investigations for uncertainty quantification in brake squeal analysis. *J. Sound Vib.* **2016**, *367*, 37−55.
(9) Butlin, T.; Woodhouse, J. A systematic experimental study of squeal initiation. *J. Sound Vib.* **2011**, *330*, 5077−5095.
(10) Chen, G. X.; Lv, J. Z.; Zhu, Q.; He, Y.; Xiao, X. B. Effect of the braking pressure variation on disc brake squeal of a railway vehicle: test measurement and finite element analysis. *Wear* **2019**, *426-427*, 1788−1796.
(11) Lee, S.; Jang, H. Effect of plateau distribution on friction instability of brake friction materials. *Wear* **2018**, *400-401*, 1−9.
(12) Lazzari, A.; Tonazzi, D.; Massi, F. Squeal propensity characterization of brake lining materials through friction noise measurements. *Mech. Syst. Signal Process.* **2019**, *128*, 216−228.
(13) Wang, D. W.; Mo, J. L.; Zhu, Z. Y.; Ouyang, H.; Zhu, M. H.; Zhou, Z. R. How do grooves on friction interface affect tribological and vibration and squeal noise performance. *Tribol. Int.* **2017**, *109*, 192−205.
(14) Zhang, Z.; Oberst, S.; Lai, J. C. S. On the potential of uncertainty analysis for prediction of brake squeal propensity. *J. Sound Vib.* **2016**, *377*, 123−132.
(15) Kang, J. Automotive brake squeal analysis with rotating finite elements of asymmetric disc in time. *J. Sound Vib.* **2017**, *393*, 388−400.
(16) Chu, Z.; Zheng, F.; Liang, L.; Yan, H.; Kang, R. Parameter determination of a minimal model for brake squeal. *Appl. Sci.* **2018**, *8*, 37.
(17) Wang, X. C.; Mo, J. L.; Ouyang, H.; Wang, D. W.; Chen, G. X.; Zhu, M. H.; Zhou, Z. R. Squeal noise of friction material with groove-textured surface: an experimental and numerical analysis. *J. Tribol.* **2016**, *138*, No. 021401.
(18) Lü, H.; Yu, D. Brake squeal reduction of vehicle disc brake system with interval parameters by uncertain optimization. *J. Sound Vib.* **2014**, *333*, 7313−7325.
(19) Magnier, V.; Brunel, J. F.; Dufrénoy, P. Impact of contact stiffness heterogeneities on friction-induced vibration. *Int. J. Solids Struct.* **2014**, *51*, 1662−1669.
(20) Oberst, S.; Lai, J. C. S.; Marburg, S. Guidelines for numerical vibration and acoustic analysis of disc brake squeal using simple models of brake systems. *J. Sound Vib.* **2013**, *332*, 2284−2299.
(21) Nouby, M.; Srinivasan, K. Simulation of the structural modifications of a disc brake system to reduce brake squeal. *Proc. Inst. Mech. Eng., Part D* **2011**, *225*, 653−672.
(22) Nouby, M.; Abdo, J.; Mathivanan, D.; Srinivasan, K. Evaluation of disc brake materials for squeal reduction. *Tribol. Trans.* **2011**, *54*, 644−656.
(23) North, M. R. Disc brake squeal. *Proc. IMechE* **1976**, *38*, 169−176.
(24) Oberst, S.; Lai, J. A Critical Review of Brake Squeal and its Treatment in Practice. *37th international congress and exhibition on noise control engineering Inter-Noise conference*; Institute of Noise Control Engineering 2008, *9*, 670−680, DOI: 10.13140/RG.2.1.2840.6160.
(25) Junior, M. T.; Gerges, S. N.; Jordan, R. Analysis of brake squeal noise using the finite element method: a parametric study. *Appl. Acoust.* **2008**, *69*, 147−162.
(26) Nishiwaki, M.; Yamamoto, Y. A Study on trigger of small friction noise in disc brake squeal. *SAE Tech. Pap.* **2018**, 0148−7191.
(27) Lyu, H.; Walsh, S. J.; Chen, G.; Zhang, L.; Qian, K.; Wang, L. Analysis of friction-induced vibration leading to brake squeal using a three degree-of-freedom model. *Tribol. Lett.* **2017**, *65*, 105.
(28) Masoomi, M.; Katbab, A. A.; Nazockdast, H. Reduction of Noise from Disc Brake Systems Using Composite Friction Materials Containing Thermoplastic Elastomers (TPEs). *Appl. Compos. Mater.* **2006**, *13*, 305−319.
(29) Bhatt, B.; Kalel, N.; Darpe, A.; Bijwe, J. Promaxon-D reinforced brake-pads to ameliorate the noise-vibration performance. *Wear* **2021**, No. 203808.
(30) Kalel, N.; Darpe, A.; Bijwe, J. Propensity to noise and vibration emission of copper-free brake-pads. *Tribol. Int.* **2020**, No. 106651.
(31) Kamioka, N.; Tokumura, H.; Yoshino, T. Friction material containing BT resin dust. US Pat. 5,384,344; 1995.
(32) Yamashita, Y.; Nakagawa, M.; Ibuki, M.; Kishimoto, H. Friction material for making brake pads. US Pat. 5,266,395; 1993.
(33) Nakagawa, M.; Yamashita, Y.; Ibuki, M.; Kishimoto, H. Friction material and method of manufacturing such material. US Pat. 5,268,398; 1993.
(34) Aranganathan, N.; Mahale, V.; Bijwe, J. Effects of aramid fiber concentration on the friction and wear characteristics of non-asbestos organic friction composites using standardized braking tests. *Wear* **2016**, *354*, 69−77.
(35) Cai, P.; Li, Z.; Wang, T.; Wang, Q. Effect of aspect ratios of aramid fiber on mechanical and tribological behaviors of friction materials. *Tribol. Int.* **2015**, *92*, 109−116.
(36) Satapathy, B. K.; Bijwe, J. Performance of friction materials based on variation in nature of organic fibres: Part I. Fade and recovery behaviour. *Wear* **2004**, *257*, 573−584.
(37) Satapathy, B. K.; Bijwe, J. Composite friction materials based on organic fibres: Sensitivity of friction and wear to operating variables. *Composites, Part A* **2006**, *37*, 1557−1567.
(38) Kim, S. J.; Cho, M. H.; Lim, D.-S.; Jang, H. Synergistic effects of aramid pulp and potassium titanate whiskers in the automotive friction material. *Wear* **2001**, *251*, 1484−1491.
(39) Kim, S. J.; Jang, H. Friction and wear of friction materials containing two different phenolic resins reinforced with aramid pulp. *Tribol. Int.* **2000**, *33*, 477−484.
(40) *PBO fiber ZYLON*; http://www.toyobo-global.com/seihin/kc/pbo/zylon-p/bussei-p/technical.pdf

(41) Aranganathan, N.; Bijwe, J. Development of copper-free eco-friendly brake-friction material using novel ingredients. *Wear* **2016**, *352-353*, 79−91.
(42) Mahale, V.; Bijwe, J.; Sinha, S. A step towards replacing copper in brake-pads by using stainless steel swarf. *Wear* **2019**, *424-425*, 133−142.
(43) Kalel, N.; Bhatt, B.; Darpe, A.; Bijwe, J. Exploration of Zylon fibers with various aspect ratios to enhance the performance of eco-friendly brake-pads. *Tribol. Int.* **2022**, No. 107385.
(44) Kim, Y. C.; Cho, M. H.; Kim, S. J.; Jang, H. The effect of phenolic resin, potassium titanate, and CNSL on the tribological properties of brake friction materials. *Wear* **2008**, *264*, 204−210.
(45) Kalel, N.; Bhatt, B.; Darpe, A.; Bijwe, J. Role of binder in controlling the noise and vibration performance of brake-pads. *J. Automob. Eng.* **2021**.
(46) Wu, Y. K.; Tang, B.; Xiang, Z. Y.; Qian, H. H.; Mo, J. L.; Zhou, Z. R. Brake squeal of a high-speed train for different friction block configurations. *Appl. Acoust.* **2021**, *171*, No. 107540.
(47) Dihua, G.; Dongying, J. A study on disc brake squeal using finite element methods. *SAE Tech. Pap.* **1998**, 0148−7191.
(48) Kung, S.; Steizer, G.; Belsky, V.; Bajer, A. Brake squeal analysis incorporating contact conditions and other nonlinear effects. *SAE Tech. Pap.* **2003**, 2003-01-3343, 2003.
(49) Massi, F.; Giannini, O. Slight effect of damping on the propensity of squeal instability: An experimental investigation. *J. Acoust. Soc. Am* **2008**, *123*, 2017.
(50) Wansu, S.; Park, J.; Choi, J.; Lee, J. J.; Jang, H. Effects of reinforcing fibers on airborne particle emissions from brake pads. *Wear* **2021**, *484-485*, No. 203996.
(51) Ma, Y.; Wu, S.; Zhuang, J.; Tong, J.; Qi, H. Tribological and physio-mechanical characterization of cow dung fibers reinforced friction composites: an effective utilization of cow dung waste. *Tribol. Int.* **2019**, *131*, 200−211.

https://doi.org/10.1021/acsomega.2c02313
ACS Omega 2022, 7, 21946−21960